Available online at www.sciencedirect.com
SCIENCE DIRECT®
ELSEVIER
Ultramicroscopy 106 (2006) 105–113
ultramicroscopy
www.elsevier.com/locate/ultramic

Determination of the mean inner potential in III–V semiconductors, Si and Ge by density functional theory and electron holography

P. Kruse[a], M. Schowalter[b,*], D. Lamoen[c], A. Rosenauer[b], D. Gerthsen[a]

[a]*Laboratorium für Elektronenmikroskopie, Universität Karlsruhe, D-76128 Karlsruhe, Germany*
[b]*Institut für Festkörperphysik, Universität Bremen, D-28359 Bremen, Germany*
[c]*TSM, Departement Fysica, Universiteit Antwerpen, B-2020 Antwerpen, Belgium*

Received 22 February 2005; received in revised form 7 June 2005; accepted 22 June 2005

Abstract

The mean inner potentials of various III–V semiconductors, Si and Ge have been calculated by density functional theory methods. For that purpose, the Coulomb potential of slabs consisting of a crystal and vacuum region has been computed and averaged inside the crystal region. The computed values are in agreement with experimental values obtained by electron holography for Si and GaAs. For the other semiconductors, the deviations are smaller than 0.8 V. The results from density functional theory are approximately 10% smaller than the values derived from atomic scattering factors computed by Hartree Fock calculations.

PACS: 73.61.Ey; 71.15.Mb; 61.14.Nm

Keywords: Mean inner potential; Density functional theory; Electron holography

1. Introduction

The fabrication of optoelectronic semiconductor devices requires the variation of chemical compositions on a nanometer scale. For the development of such devices, quantitative measurement of chemical compositions on an atomic scale is needed. Transmission electron microscopy (TEM) has reached the state to supply such information [1].

One possible approach is based on the exploitation of a chemical sensitive reflection as, for example, the [0 0 2] reflection for materials with sphalerite structure. Due to the dynamical scattering process, the amplitude of the [0 0 2] reflection is not only depending on the chemical composition, but on the thickness of the specimen as well.

*Corresponding author.
E-mail address: schowalter@ifp.uni-bremen.de (M. Schowalter).

0304-3991/$ - see front matter © 2005 Elsevier B.V. All rights reserved.
doi:10.1016/j.ultramic.2005.06.057

Electron holography provides a method for the determination of the local specimen thickness that is based on the mean inner crystal potential (MIP). Thus, an accurate knowledge of the MIP is needed for chemical analysis based on the [0 0 2] reflection [2]. Chemical information can also be gained by measuring the phase shift of the undiffracted beam by electron holography, if the MIPs of the involved materials are sufficiently different and if they are known with sufficient accuracy.

The MIP is defined as the average Coulomb potential within the crystal, where the zero point of the Coulomb is chosen in the vacuum at infinite distance from the crystal. Such a definition reflects the experimental situation in a microscope, where an electron starts from at nearly infinite distance from a specimen and traverses the specimen. The first numerical estimates of the MIP were given by Bethe [3]. He expressed the MIP in terms of the second moment of the charge density for spherical atoms and made a first estimate of the value of the MIP for Ni using the H-atom eigenfunctions and "Abschirmungszahlen" for the core electrons as well as the assumption that the conduction electrons are smeared out homogenously over the crystal. He found a value of 18.93 V, which overestimated the experimental value of 14.8 V [4]. He noted that the deviation is most likely due to the charge distribution, which was not known accurately. Another analytical method of calculating MIPs was used by Sánchez and Ochando [5]. They used an analytical expression with fit parameters which they fitted to crystallographic data of isolated atoms. In 1958, Ibers [6] found a relation between the MIP and the electron scattering factors at zero scattering angle. His relationship has been used widely for derivation of the MIP for different materials, because it gave an easy method to derive approximate values of the MIP. Using the approximation of Ibers [6], the MIP is calculated by a superposition of the scattering factors in forward direction of unbound atoms i in the unit cell of volume Ω_c,

$$V_0 = \frac{\hbar^2}{2\pi m e\,\Omega_c} \sum_i f^i_{el}(0), \tag{1}$$

where $\hbar$ is Planck's constant, m the electron mass and e the charge of the electron. The atomic scattering factors $f^i_{el}(0)$ are computed from isolated atoms [7] and do not include bond effects (we will later refer to this method as the isolated atom approximation). Bonds give rise to a redistribution of charge and to a slowly varying part of the potential. This influences strongly the scattering factors for low scattering angles. Especially, the MIP as the zero Fourier component of the Coulomb potential is affected. To obtain values for the MIP that are more accurate, the charge distribution and the crystal potential have to be computed for the full crystal, also taking into account redistribution of charge in chemical bonds. The first computations taking into account the redistribution of electrons were performed by Kim et al. [8]. They computed the charge distribution of crystals self-consistently within the density functional theory (DFT) approach and derived the MIP from these data. The MIPs obtained in this work were in good agreement with experimental values published recently (Kruse et al. [9]).

In this paper, we have calculated the MIPs of various III–V semiconductors, Si and Ge by DFT methods. Experimental values of the MIPs for GaAs, InAs, GaP and InP obtained by electron holography were already published in Ref. [9]. Here, we additionally provide experimental values for Si and GaSb. These measurements were performed in analogy to those described in [9]. Therefore, only a brief description of the experimental approach is given in the following.

2. Experimental approach

When an electron wave passes through a crystal, it is accelerated by its MIP. This leads to a shortening of the wavelength within the crystal, which can be described by a refractive index larger than one, because the MIP is a positive quantity. Therefore, the phase of the electron wave penetrating through the crystal is shifted with respect to a reference wave travelling in vacuum.

Additional phase shifts arise due to charging of the specimen and dynamic diffraction of the electron wave. In the TEM experiment, the former can be excluded for conducting materials. To keep the phase shift from dynamic diffraction small, the

specimen orientation was chosen in such a way that a strong excitation of reflections is avoided. Remaining dynamical effects were included by Bloch-wave calculations as described in detail in Ref. [9].

In the high energy limit and in absence of the mentioned dynamical diffraction effects the phase shift $\Delta\varphi$ is proportional to the mean inner potential V_0 and to the thickness t of the specimen:

$$\Delta\varphi = C_E V_0 t. \quad (2)$$

The constant of proportionality C_E is weakly depending on the accelerating voltage U_{acc} of the electron microscope and can be calculated [10] according to

$$C_E = \frac{1}{\hbar}\frac{e^2 U_{acc}/c^2 + em}{\sqrt{(eU_{acc}/c)^2 + 2eU_{acc}m}}. \quad (3)$$

In an electron holography experiment, the electron object wave penetrating through the specimen interferes with the electron wave passing through vacuum. The phase shift $\Delta\varphi$ is measured from a Fourier analysis of the interference pattern and the MIP is obtained from Eq. (2), as described in Refs. [10,9].

3. Theoretical approach

3.1. Introduction

The solution of the Schrödinger equation of the crystal including the bonds is a non-trivial task as a change in the electronic charge density affects the potential and thereby the charge distribution itself. At present, this problem has only been solved approximately and one successful approach is the DFT formalism. It is derived from the fact that any physical quantity can be expressed as a unique functional of the charge density. Therefore, any physical quantity can be calculated from the charge density, if the associated functional is known. To obtain the charge density, Schrödinger-like equations, the Kohn Sham equations, have to be solved self-consistently. The Hamiltonian of the Kohn Sham equations consists of the traditional kinetic part, the Coulomb part and an additional part, which takes into account the exchange and correlation effects. This part is called the exchange and correlation potential V_{XC}. Several approximations exist for V_{XC}. The most common one is the local density approximation (LDA), where the local exchange and correlation potential is found under the assumption, that the charge density of the local position is constant over the whole crystal. Other approximations are the generalized gradient approximations (GGA), which take into account the gradients of the charge density. For our computations, we used the GGA of Perdew et al. [11] within the WIEN2k package [12]. The general solution of the Kohn Sham equations start with the calculation of an initial charge density. With the help of the Poisson equation the associated potentials can be calculated. Using these, the Kohn Sham are solved, resulting in Kohn Sham electron wave functions, from which a new electron charge density can be obtained. The procedure is repeated until the charge distribution reproduces itself and self-consistency is reached.

3.2. Applied procedure

For the determination of the MIP the potential distribution of a supercell structure as depicted in Fig. 1 was calculated. It consists of a crystal slab with (1 1 0) surfaces, that is separated by vacuum layers from the neighboring slabs in the periodic continuation. For the calculations, the full potential linearized augmented plane wave method as implemented in the WIEN2k package [12] was used. After the DFT calculation the Coulomb

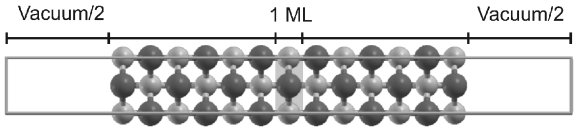

Fig. 1. GaAs supercell with (1 1 0) surfaces in [0 0 1]-projection consisting of 13 monolayers thickness and 1.5 nm vacuum. The extension of the supercell is marked with a gray frame. The Coulomb potential is averaged in the gray underlaid region, the origin of the Coulomb potential is chosen in the center of the vacuum region. Due to the periodic border conditions, the center of the vacuum region corresponds to the left (or right) border of the cell.

potential was averaged in the central monolayer (ML), because it represents the bulk properties best. The region used for averaging is indicated with a gray rectangle in Fig. 1 and enlarged in Fig. 2. Within the central region, the MIP is calculated for different subregions. In each of these subregions, the potential is described by a respective set of basis functions. The WIEN2k code uses two kinds of basis functions: spherical harmonics inside muffin tin spheres of radius R_{MT} and of volume Ω^{MT} around the atom positions and plane waves in the remaining interstitial subregion. The MIP contributions $V_0^{R_{\mathrm{MT}}}$ of the muffin tin spheres, shown as gray colored discs in Fig. 2, are determined via

$$V_0^{R_{\mathrm{MT}}} = \frac{3}{R_{\mathrm{MT}}^3 Y_{00}} \sum_i [r^2 V_{00}(r)]_i \Delta r_i, \tag{4}$$

where r is the distance from the atom position, $V_{00}(r)$ is the radial potential distribution to the spherical harmonic Y_{lm} with $l = m = 0$. Contributions from spherical harmonics with $l > 0$ vanish due to the orthogonality relations of the spherical harmonics, if the potential of a whole muffin tin sphere is averaged. In our setup, this is the case for an odd number of MLs and a width of the averaged region of one ML. In the case of an even number of MLs and a width of the central crystal region of one ML, it contains half rows of muffin tin spheres at the left and right borders. In this case, either the volume used for the averaging has to be increased to two MLs, or the spherical harmonics with $l = 1$ have to be taken into account.

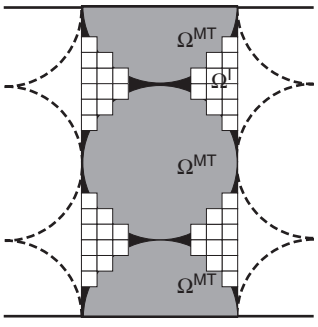

Fig. 2. Sketch of the shaded region of Fig. 1. The potential in the muffin tin spheres Ω^{MT} is averaged according to Eq. (4) on the basis of the radial potential distribution. The region Ω^{I} corresponds to the squares with their centers outside the spheres. Regions that correspond to neither Ω^{MT} nor Ω^{I} are marked black.

In the volume Ω^{I} of the interstitial region, the potential distribution was averaged on an almost cubic grid with a sampling density n_{L}. The volume Ω^{I} and the sampling grid are indicated by a mesh in Fig. 2. The size of the grid was set up by distorting a cubic grid in such a way that the whole supercell could be filled by an integer number of meshpoints in every dimension.

Due to the different samplings in the muffin tin and the interstitial subregions, the volumes Ω^{MT} and Ω^{I} are not complementary. Instead, individual elements of the mesh may overlap with the muffin tin spheres, and there are parts of the interstitial region that neither belong to the muffin tin spheres nor to any element of the mesh. Therefore, we define a defect volume $\Omega^{\mathrm{S}} := \Omega^{\mathrm{C}} - (\Omega^{\mathrm{MT}} + \Omega^{\mathrm{I}})$ that describes the deviation between $\Omega^{\mathrm{MT}} + \Omega^{\mathrm{I}}$ and the volume Ω^{C} of the supercell. The volume Ω^{S} corresponds to those parts close to the surface of the muffin tin spheres that either were not taken into account (positive contribution to Ω^{S}) or which were taken into account twice (negative contribution to Ω^{S}). Because this volume consists of parts that are lying close to the border of the muffin tin spheres, it is taken into account with the mean potential at the surface of the muffin tin spheres. The contribution of Ω^{S} vanishes with increasing sampling density n_{L} of the interstitial subregion, but its incorporation increases the convergence of the MIP with respect to n_{L}, and thereby significantly saves computation time. The total MIP was calculated by the sum of the MIPs within the three different subregions, weighted by their respective volume parts

$$V_0 = \frac{1}{\Omega^{\mathrm{C}}} [V_0^{R_{\mathrm{MT}}} \Omega^{\mathrm{MT}} + V_0^{\mathrm{I}} \Omega^{\mathrm{I}} + V_0(r = R_{\mathrm{MT}}) \Omega^{\mathrm{S}}] - V_{\mathrm{Vac}}. \tag{5}$$

The region within the supercell that was used to obtain the potential V_{Vac} was chosen at the largest possible distance from the crystal slabs, which is the central position of the vacuum layer. Due to the periodic continuation of the supercell, the center of the vacuum region corresponds to the left (or right) border of the supercell (see Fig. 1).

3.3. Parameter optimization

Note that all calculated materials have sphalerite (or diamond) crystal structure. As it can already be seen in the free atom approximation from Eq. (1), the MIP depends on the volume of the unit cell and, thus on the lattice parameter. The lattice parameters used are listed in Table 1 together with the radii of the muffin tin spheres. The radii were chosen to obtain nearly touching spheres. For the supercells of the III/V semiconductors, the radii were chosen to have the same size for both the group III and the group V elements.

Since the MIP is defined with respect to a zero point of the Coulomb potential at infinite distance from the crystal, the MIP has to be converged with respect to the size of the vacuum region in the slab in order to assure that the vacuum region is large enough. The points lying on the solid line in Fig. 3 display the results of computations of the MIP as a function of the size of the vacuum region. It can be seen that the MIP is well converged already for 1 nm vacuum. However, for further computations 1.5 nm vacuum were chosen to assure that the MIP is converged well enough. The MIP is a quantity referring to bulk material and therefore, the influence of the surface on the charge distribution in the innermost ML of the slab, where the Coulomb potential is averaged, has to be minimized. We checked this by computing the MIP for GaAs slabs with different number of MLs for a fixed size of the vacuum layer of 1.5 nm. The results are shown as crosses on the dashed line in Fig. 3 and it was found that the MIP is converged well for slabs consisting of 13 ML GaAs.

Table 1
Lattice constants and muffin tin radii used for the calculations

Material	a (nm)	R_{MT} (nm)
Si	0.54311	0.1175
Ge	0.565791	0.1224
AlP	0.54635	0.1182
GaP	0.5449	0.1179
InP	0.5868	0.1270
AlAs	0.5661	0.1225
GaAs	0.56536	0.1224
InAs	0.6058	0.1311
AlSb	0.61355	0.1328
GaSb	0.6095	0.1319
InSb	0.6479	0.1402
AlN	0.436	0.0943
GaN	0.452	0.0978
InN	0.498	0.1078

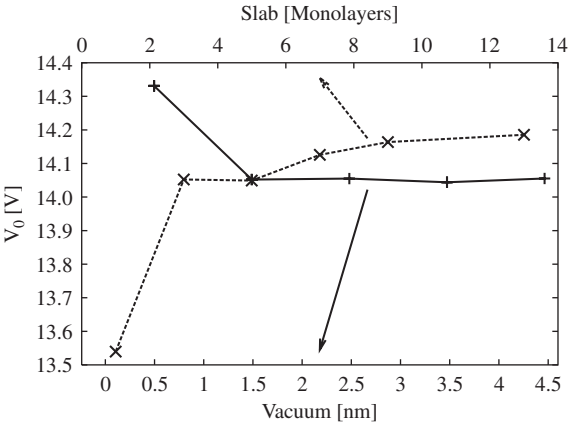

Fig. 3. The dependence of the MIP with respect to the thickness of the crystal slab (1.5 nm vacuum) and the thickness of the vacuum layer (3 ML GaAs) that is separating the crystal slabs.

In addition, several parameters within the WIEN2k code control the convergence of the calculated quantities. Their effects on the MIP were tested for supercells with 3 or 7 MLs GaAs and 0.5 or 1.5 nm vacuum. Small geometries of slabs were used in order to keep computation time reasonably small. Here, we assume that the precision of a parameter, for which the MIP was converged to a certain precision, does not depend on the size of the supercell used in the DFT calculation.

The DFT calculation provides charge and potential distributions in a Fourier representation. The spatial frequencies used are limited by the cutoff parameter g_{Max}. Its effect on the MIP is depicted in Fig. 4 as dashed line. The MIP is well converged for a cutoff parameter of $14\sqrt{Ry}$.

The accuracy of the wave functions is limited by the number of sampling points k within the first Brillouin zone. The effect of the k point sampling on the MIP is demonstrated as solid line in Fig. 4. The value of the MIP is well converged for 64 k points in the full Brillouin zone.

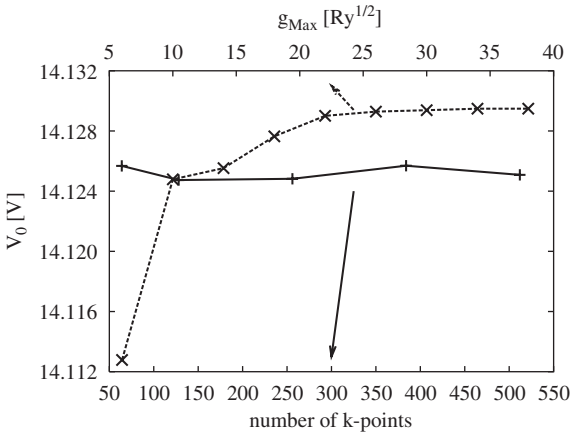

Fig. 4. The MIP in dependence of the maximum spatial frequency g_{Max} of the potential (3 ML GaAs/0.5 nm vacuum) and the number of k-points in the first Brillouin zone (7 ML GaAs/1.5 nm vacuum).

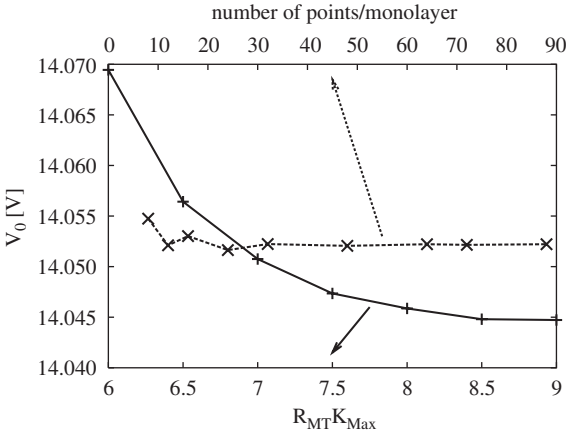

Fig. 5. The dependence of the MIP (3 ML GaAs/1.5 nm vacuum) with respect to the number of sampling points in the interstitial region and in dependence of K_{Max}.

The maximum allowed spatial frequency for the Fourier expansion of the basis set in the interstitial region K_{Max} also limits the accuracy of the computation of the MIP. Since the size of the interstitial region depends on the used muffin tin radius, the numbers of plane waves necessary to describe the Kohn Sham orbitals in the interstitial region also depends on the muffin tin radius. Therefore, the product of the maximum spatial frequency K_{Max} and the muffin tin radius R_{MT} is used as input parameter in the WIEN2k code. The MIP as a function of $K_{\mathrm{Max}}R_{\mathrm{MT}}$ is shown in Fig. 5 as solid line. A value of about $K_{\mathrm{Max}}R_{\mathrm{MT}} = 7.0$ is sufficient to converge the MIP.

After the DFT calculation, the potential is averaged in the subregions. While a maximum accuracy for the muffin tin subregion is reached by evaluating Eq. (4) directly, the interstitial region has to be sampled with sufficient density. The dependence of the evaluated MIP on the number of sampling points per ML is shown as dashed line in Fig. 5. A sampling of $48^3/\mathrm{ML}^3$ points was sufficient to converge the MIP.

3.4. Estimation of errors

On the basis of the parameter variation, the errors resulting for a parameter set with acceptable requirements of computation time for the DFT calculation have been estimated. These parameters are:

- orientation of the surface {1 1 0},
- thickness of the crystal slab 13 ML,
- thickness of the vacuum region 1.5 nm,
- $g_{\mathrm{Max}} = 14\sqrt{Ry}$,
- $R_{\mathrm{MT}}K_{\mathrm{Max}} = 7$,
- 64 k-points in the full Brillouin zone,
- $48^3/\mathrm{ML}^3$ sampling points for the evaluation of the MIP in the interstitial region.

The relative error that is caused by using this set of parameters is estimated as follows.

The most significant errors arise due to the finite size of the slab thickness and the vacuum region. While the MIP fluctuates for vacuum thicknesses larger than 1.5 nm with a relative error of 8×10^{-4}, the exponential extrapolation of MIPs with the four highest thicknesses results in a relative error of 6×10^{-4}.

For the remaining parameters errors were computed by taking the maximum deviation of the MIP computed for larger parameters than the converged parameter. The maximum frequency of the plane wave expansion of the potential was chosen to $g_{\mathrm{Max}} = 14\sqrt{Ry}$, thus, contributing a

relative error of 3×10^{-4}. The expansion of the Kohn Sham electron wave functions was limited by a maximum frequency of $R_{MT}K_{Max} = 7$ with a density of 64 k-points in the full Brillouin zone and thus contributes errors of 3.6×10^{-4} and 7×10^{-5}, respectively. The averaging in the interstitial was done with a sampling density of $48^3/ML^3$ and thus contributes a relative error of 1.1×10^{-5}. These errors sum up to a relative error of 2.1×10^{-3} for GaAs for example, corresponding to an absolute error of 30 meV.

4. Results

Using the parameters listed at the end of the preceding section, the MIPs for various III–V semiconductors with sphalerite structure were computed. The results are listed in Table 2 together with the MIPs computed by Eq. (1), using electron atomic scattering factors derived from Hartree Fock (HF) calculations [7]. The table also provides experimental values from literature and the experimental values for Si and GaSb obtained in this work.

Additionally, the MIP of GaAs has been computed to 14.99 V from the potential distribution of free atoms, that was calculated in relativistic local spin density approximation (LSDA). This atomic density is used as the starting density of the DFT calculation and does not include bond effects.

5. Discussion

Fig. 6 gives an overview of MIPs determined by DFT, HF and experiment. The MIPs determined using DFT are in general 10% smaller than MIPs calculated using the HF. This reduction is due to two components that can be separated by the MIP of GaAs obtained in atomic LSDA (14.99 V): the use of the DFT instead of the HF theory effect 25% of the reduction and the inclusion of bonds effect the remaining 75% of the reduction.

The comparison of the MIP of Si from DFT and experiment show an agreement for the values found here and by Wang et al. [14] as well as with

Table 2
MIPs resulting from DFT, Hartree Fock (HF) and experiment

Material	V_0 (V)	V_0^{EMS} (V)	V_0^{Exp} (V)
Si	12.57	13.91	12.52 ± 0.71★; 9.26 ± 0.08 [10]★; 11.5 ± 0.5 [13]★; 12.1 ± 1.3 [14]★
Ge	14.67	15.58	14.3 ± 0.2 [15]★; 15.6 ± 0.8 [16]$^{\gamma}$
AlP	11.39	13.34	–
GaP	13.63	14.88	14.38 ± 0.12 [9]★; 12.2 [17]†
InP	13.90	15.06	14.53 ± 0.07 [9]★
AlAs	12.34	13.93	–
GaAs	14.19	15.26	14.24 ± 0.08 [9]★; 14.53 ± 0.17 [10]★; 13.2 [17]†
InAs	14.34	15.26	14.50 ± 0.08 [9]★
AlSb	12.89	13.96	–
GaSb	14.45	15.27	14.08 ± 0.05★
InSb	14.28	15.05	–
AlN	14.23	18.67	–
GaN	16.82	19.30	–
InN	17.35	19.57	–

The DFT calculations were done for slabs of 13 MLs thickness with (1 1 0) surfaces and separated by a vacuum layer of 1.5 nm thickness. The experimental values are obtained by electron holography★, RHEED† or interferometry$^{\gamma}$. The uncited experimental values for Si and GaSb have been determined by the authors analogously to former measurements presented in Ref. [9].

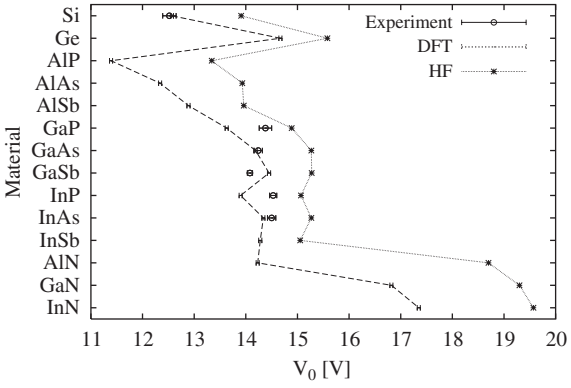

Fig. 6. Resulting MIPs from DFT, HF and experiment according to Table 2. Adjacent data points from DFT and HF are connected by a guiding line.

the earlier calculations of Kim et al. [8], when one takes into account the error for a slab thickness of 6 ML, which was used by Kim et al. [8]. The MIP of Si measured by Gajdardziska et al. [10] deviates by about a factor of $\frac{1}{\sqrt{2}}$ from the MIP presented here.

The MIPs of Ge obtained by DFT and holographic experiments on cleaved wedges [15] are in close agreement, in contrast to the 1 V larger results from holographic experiments on samples with parallel surfaces [16], whose accuracy is probably limited by the measurement of the absolute specimen thickness.

For GaAs there is agreement with the experimental values of Kruse et al. [9] and a deviation of 0.34 V to the value of Gajdardziska et al. [10]. A larger deviation of 0.99 V is found for a comparison to the RHEED measurement by Yamamoto and Spence [17]. The deviation between experimental and DFT values is 0.37 V for GaSb.

The MIP of InAs computed by DFT only slightly deviates from the measurement of Kruse et al. [9]. The difference of the MIPs of InAs and GaAs is small, so that the phase of the undiffracted beam in a TEM experiment is nearly independent of the In-concentration for unstrained materials. However for the measurement of the specimen thickness by electron holography in strained In_xGa_{1-x} As semiconductor compounds, volume effects according to Eq. (1) have to be taken into account.

The phosphide system shows deviations between DFT and experiment of 0.75 V for GaP and 0.63 V for InP, which are larger than for the arsenide system. We suppose, that the accuracy of the experimental data is limited by the brittleness of GaP and InP, so that cleaved specimens exhibit wedge angles deviating from 90°. Since specimens with larger angles are mechanically more stable, the investigated specimens could have a tendency towards angles larger than 90° in the tip region, which would be connected with an underestimation of the specimen thickness and an overestimation of the measured MIP.

For the nitrides a high mean inner potential is found. These materials have a significantly smaller lattice parameter and therefore a larger MIP due to the dependence of the MIP on the volume (Eq. (1)). Compared to GaAs a two times larger MIP for GaN could be expected from the volume effect (Eq. (1)), but the smaller atomic electron scattering of the N atom lowers the MIP. While GaN and InN show a reduction of 12% and 13%, the MIP of AlN deviates by 24% from the HF values. It has to be mentioned that the latter showed a bad convergence behavior during the calculation. The bad convergence behavior may be caused by the fact that the sphalerite crystal structure is not the equilibrium crystal structure of the nitrides, which is the wurtzite structure. Therefore, the local minimum of the charge distribution could be shallow which could make the convergence difficult.

6. Conclusion

In summary, the MIP from HF calculations of free, isolated atoms is overestimated in average by 7.5% due to the neglect of the bonds and to additional 2.5% due to the neglection of the correlation effects with respect to the DFT. For the calculation of the MIP, a supercell structure is required, that consists of crystal slabs with 13 MLs thickness, separated by 1.5 nm vacuum. With such a structure, the MIP was determined with a relative error of 2.1×10^{-3}. Theory and experiment are in good agreement for Si and GaAs, small deviations were encountered for InAs (0.16 V) and GaSb (0.37 V), and larger deviations occurred for InP (0.63 V) and GaP (0.75 V).

Acknowledgements

P. K. acknowledges the Deutsche Forschungsgemeinschaft for financial support under Contract no. R02057/3.

References

[1] A. Rosenauer, Transmission Electron Microscopy of Semiconductor Nanostructures—An Analysis of Composition and Strain State, Springer Tracts in Modern Physics, vol. 182, Heidelberg, Springer, 2003.
[2] A. Rosenauer, D. Gerthen, D. Van Dyck, M. Arzberger, G. Böhm, G. Abstreiter, Ultramicroscopy 88 (2001) 51.
[3] H. Bethe, Ann. Physik 87 (1928) 55.

[4] C. Davisson, L.H. Germer, Phys. Rev. 30 (1927) 705.
[5] A. Sanchez, M.O. Ochando, J. Phys. C 18 (1985) 33.
[6] J.A. Ibers, Acta Cryst. 11 (1958) 178.
[7] P. Doyle, P.S. Turner, Acta Cryst. A 24 (1968) 390.
[8] M.Y. Kim, J.M. Zuo, J.C.H. Spence, Phys. Status Solidi A 166 (1998) 445.
[9] P. Kruse, A. Rosenauer, D. Gerthsen, Ultramicroscopy 96 (2003) 11.
[10] M. Gajdardziska-Josifovska, M.R. McCartney, W.J. de Ruijter, D.J. Smith, J.K. Weiss, J.M. Zuo, Ultramicroscopy 50 (1993) 285.
[11] J.P. Perdew, K. Burke, M. Ernzerhof, Phys. Rev. Lett. 77 (1996) 3865.
[12] P. Blaha, K. Schwarz, G.K.H. Madsen, D. Kvasnicka, J. Luitz, Wien2k, An Augmented Plane Wave + Local Orbitals Program for Calculating Crystal Properties (Karlheinz Schwarz, Tech. Universität Wien, Austria), 2001. ISBN 3-9501031-1-2, 2001.
[13] L. Wu, M.A. Schofield, Y. Zhu, J. Tafto, Ultramicroscopy 98 (2004) 135.
[14] Y.C. Wang, T.M. Chou, M. Libera, T.F. Kelly, Appl. Phys. Lett. 70 (1997) 1296.
[15] J. Li, M.R. McCartney, R.E. Dunin-Borkowski, D.J. Smith, Acta Cryst. A 55 (1999) 652.
[16] H. Hoffmann, C. Jonssen, Z. Physik 182 (1965) 360.
[17] N. Yamamoto, J.C.H. Spence, Thin Solid Films 104 (1983) 43.